Received: 28 September 2024 | Revised: 14 November 2024 | Accepted: 27 November 2024

DOI: 10.1096/fj.202402292R

RESEARCH ARTICLE

The FASEB Journal

To activate NAD(P)H oxidase with a brief pulse of photodynamic action

Xiao Bing Xie | **Yu Shu** | **Zong Jie Cui**

College of Life Sciences, Beijing Normal University, Beijing, China

Correspondence
Zong Jie Cui, College of Life Sciences, Beijing Normal University, Beijing 100875, China.
Email: zjcui@bnu.edu.cn

Funding information
The Natural Science Foundation of China, Grant/Award Number: 32271278

Abstract

Reduced nicotinamide adenine dinucleotide phosphate [NAD(P)H] oxidases (NOX) are a major cellular source of reactive oxygen species, regulating vital physiological functions, whose dys-regulation leads to a plethora of major diseases. Much effort has been made to develop varied types of NOX inhibitors, but biotechnologies for spatially and temporally controlled NOX activation, however, are not readily available. We previously found that ultraviolet A (UVA) irradiation activates NOX2 in rodent mast cells, to elicit persistent calcium spikes. NOX2 is composed of multiple subunits, making studies of its activation rather complicated. Here we show that the single-subunit nonrodent-expressing NOX5, when expressed ectopically in CHO-K1 cells, is activated by UVA irradiation (380 nm, 0.1–12 mW/cm^2, 1.5 min) inducing repetitive calcium spikes, as monitored by Fura-2 fluorescent calcium imaging. UVA-elicited calcium oscillations are inhibited by NOX inhibitor diphenyleneiodonium chloride (DPI) and blocked by singlet oxygen ($^1O_2$) quencher Trolox-C (300 μM). A brief pulse of photodynamic action (1.5 min) with photosensitizer sulfonated aluminum phthalocyanine (SALPC 2 μM, 675 nm, 85 mW/cm^2) in NOX5-CHO-K1 cells, or with genetically encoded protein photosensitizer miniSOG fused to N-terminus of NOX5 (450 nm, 85 mW/cm^2) in miniSOG-NOX5-CHO-K1 cells, induces persistent calcium oscillations, which are blocked by DPI. In the presence of Trolox-C, miniSOG photodynamic action no longer induces any calcium increases in miniSOG-NOX5-CHO-K1 cells. DUOX2 in human thyroid follicular cells SW579 and in DUOX2-CHO-K1 cells is similarly activated by UVA irradiation and

Abbreviations: $^1O_2$, singlet oxygen; AlPcS4, tetrasulfonated aluminum phthalocyanine; BSA, bovine serum albumin; CaMBD, calmodulin-binding domain; CCD, charge-coupled device; CHO-K1, Chinese hamster ovary K1 cell line; DMEM, Dulbecco's Modified Eagle Medium; DPI, diphenyleneiodonium chloride; DUOX2, dual NAD(P)H oxidase 2; ER, endoplasmic reticulum; FAD, flavin adenine dinucleotide; FBS, fetal bovine serum; FICZ, 6-formylindolo[3,2-b]carbazole; FMN, flavin mononucleotide; GEPP, genetically encoded protein photosensitizer; IP_3R, inositol-1,4,5-trisphosphate receptor; LED, light-emitting diode; miniSOG, mini-singlet oxygen generator; NAD, β-nicotinamide adenine dinucleotide; NAD(P)H, reduced nicotinamide adenine dinucleotide phosphate; NADP, NAD phosphate; NOX1-5, NAD(P)H oxidase 1-5; NSFC, The Natural Science Foundation of China; $O_2^{\cdot-}$, superoxide anion; PBS, phosphate-buffered saline; PhosR, phosphorylatable region; PLC, phospholipase C; PM, plasma membrane; PBR, polybasic region; PTI, Photon Technology International; REFBD, regulatory EF-binding domain; ROS, reactive oxygen species; RTK, receptor tyrosine kinase; SALPC, sulfonated aluminum phthalocyanine; TM1-7, transmembrane domain 1–7; TRITC, tetramethylrhodamine isothiocyanate; UVA, ultraviolet A.

Xiao Bing Xie and Yu Shu contributed equally to this study.

SALPC photodynamic action. These data together suggest that NOX is activated with a brief pulse of photodynamic action.

KEYWORDS

calcium oscillations, DUOX2, mini-singlet oxygen generator (miniSOG), NAD(P)H oxidase 5 (NOX5), photodynamic action, sulfonated aluminum phthalocyanine (SALPC), SW579, ultraviolet A (UVA)

1 | INTRODUCTION

Reduced nicotinamide adenine dinucleotide phosphate (NADPH), produced by multiple metabolic pathways,[1,2] is oxidized by NAD(P)H oxidase (NOX1-5) or dual NOX1,2 (DUOX1,2) to produce superoxide anion ($O_2^{\cdot-}$) or hydrogen peroxide (H_2O_2).[3–7] The NOX isoenzymes are a major source of cellular reactive oxygen species (ROS), to regulate innate immunity, cell signaling, chromatin remodeling and gene expression, stem cell maintenance and differentiation, cell death, organ development, and aging.[1,8–10] Dysregulated reactive oxygen species (ROS) generation leads to a plethora of diseases including atherosclerosis, hypertension, diabetic nephropathy, lung fibrosis, neurodegenerative diseases, and cancer.[6,11–13] Much effort has been made in the research and development of both pan-NOX and type-specific NOX inhibitors.[14,15] Technologies for spatially and temporally controlled activation of NOX are, however, not readily available.

The ultraviolet A band (UVA, 320–400 nm) in solar radiation penetrates the skin to the dermis, reaching dermal fibroblasts, keratinocytes, vascular endothelial cells, and mast cells.[16–20] We have found previously that UVA irradiation activates the multi-subunit NOX2 ($gp91^{Phox}$) in rodent mast cells (rat peritoneal mast cells, mouse bone marrow-derived mast cells, and rat mast cell line RBL-2H3), to trigger persistent calcium oscillations and IL6/LTC4 release, via the $O_2^{\cdot-}$-receptor tyrosine kinase–phospholipase Cγ–IP_3–IP_3 receptors (IP_3R)–Ca^{2+} signaling pathway.[21,22] The NOX2 holoenzyme is composed of catalytic NOX2 and accessory subunits (transmembrane P22, cytosolic P40, P47, P67, Rac),[3,4,23] rendering the detailed study of NOX2 activation by UVA rather complicated, but the rodent non-expressing single subunit NOX5[5,24,25] seems much better suited for mechanistic investigations due to simplicity in holoenzyme composition.

Mammalian cells are endowed with multiple endogenous UVA-absorbing photosensitizers, such as flavin mononucleotide (FMN), flavin adenine dinucleotide (FAD), β-nicotinamide adenine dinucleotide (NAD), NAD phosphate (NADP), tryptophan-derived 6-formylindolo[3,2-b] carbazole (FICZ), porphyrins and riboflavin,[26–28] which would undergo UVA-driven type II photodynamic action.[27–30] NOX5 contains both NAD(P)H- and FAD-binding regions in the cytosolic C-terminal dehydrogenase domain.[3,31] The NOX isoenzyme once activated, one electron is sequentially transferred from NAD(P)H to FAD in the C-terminal domain, then on to the 2 His pairs-binding heme molecules in the transmembrane domain, and eventually to an extracellular or intraphagosomal molecule of O_2 to produce a superoxide anion ($O_2^{\cdot-}$).[24,32–34]

Were NAD(P)H and FAD coordinately bound in the NOX protein microenvironment to absorb UVA photons to initiate photodynamic action for NOX activation, would photodynamic action with external photosensitizers similarly activate the NOX isozyme? The chemical photosensitizer sulfonated aluminum phthalocyanine (SALPC/AlPcS4)[35,36] (λ_{ex} Sorret band 350 nm, Q band 675 nm, $\phi^1O_2 = 0.38$),[37,38] and the genetically encoded protein photosensitizer (GEPP) miniSOG with coordinately bound FMN (λ_{ex} 450 nm, $\phi^1O_2 \geq 0.03$),[39–41] could be used for possible photodynamic activation of NOX5.

Therefore in this work, the human NOX5 was expressed in Chinese hamster ovary K1 (CHO-K1) cells, and the effect of UVA irradiation and photodynamic action (photosensitizers SALPC and miniSOG) were examined. Possible activation by UVA irradiation and photodynamic action of DUOX2 in the human thyroid follicular epithelial cell line SW579 (expressing high levels of DUOX2) and in CHO-K1 cells ectopically expressing DUOX2 was also examined. A brief pulse (1.5 min) of both UVA irradiation and photodynamic action was found to activate both NOX5 and DUOX2, to elicit persistent calcium oscillations. This novel photodynamic biotechnology would provide a useful toolkit for the functional manipulation of NOX5, DUOX2, and possibly other NOX isoenzymes in the future.

2 | MATERIALS AND METHODS

2.1 | Materials

NOX inhibitors diphenyleneiodonium chloride (DPI, #D2926) and VAS2870 (#492000-M), $^1O_2$ quencher Trolox-C (#238813), NADPH (#N1630), and FAD (#F6625) were

bought from Sigma-Aldrich (RRID: SCR.008988, St Louis, MO, USA). Mixed Dulbecco's Modified Eagle Medium and F12 medium (DMEM/F12) (1/1) (#C11330500BT) and trypsin 0.25% (#25200056) were purchased from Invitrogen (RRID: SCR.008410, Shanghai, China). Leibovitz's L-15 medium (#PM151010) was from Procell (Wuhan, China). Rabbit anti-NOX5 primary antibody (#ab191010) and donkey anti-rabbit secondary antibody conjugated with tetramethylrhodamine isothiocyanate (TRITC) (#ab6799), rabbit anti-DUOX2 (#ab97266) primary antibody and secondary antibody Alexa Fluor® 488 goat anti-rabbit IgG (#ab150077), were all purchased from Abcam (RRID: SCR.012931, Cambridge, UK). Rabbit anti-DUOXA2 primary antibody (#PC23964S) was from Abmart (RRID: AB-3665428, Shanghai, China), goat anti-rabbit secondary antibody (IgG) conjugated with Alexa Fluor@568 (#ab175471) were also from Abcam (RRID: SCR.012931, Cambridge, UK). The plasmid *pc*DNA$^{3.1+}$*NOX5* (*NOX5*, AF353088, #69354) was from AddGene (RRID: SCR.002037, Bristol, UK). The plasmid *pKillerRed*$_{mem}$ which we re-named *pKillerRed*$_{PM}$ for its plasma membrane (PM) localization was purchased from Evrogen (#FP966) (Moscow, Russia). Plasmid *pCMV3-DUOX2* (#HG18317-UT, NCBI code NM_014080.4) was purchased from Sino Biological (Beijing, China). Tetrasulfonated aluminum phthalocyanine (AlPcS4, $C_{32}H_{16}AlClN_8O_{12}S_4$, which we named SALPC for consistency with past publications) was bought from Frontier Scientific Inc. (RRID: SCR.000914, West Logan, UT, USA) or from Luminescence Technology Corp. (LumTech, #LT-D2014) (New Taipei City, Taiwan, China). Ultrapure grade Fura-2 AM in anhydrous dimethylsulfoxidae (DMSO) (1 mM) (#21021) was bought from AAT Bioquest (Sunnyvale, CA, USA). Cell-Tak (#354241), the cell adhesive for cell attachment to cover slips, was bought from BD Bioscience (RRID: SCR.013311, Bedford, MA, USA); alternatively, Matrix-gel was used (#C0372) (Beyotime, Shanghai, China). The cell transfection reagent jetPRIME® (#101000046) was bought from Polyplus-Transfection (Illkirch, France). Kit for plasmid extraction (#DP118) was bought from TianGen Biochemicals (Beijing, China). Heme (#SR3331) was bought from Harveybio (Beijing, China).

2.2 | Cell culture

A growing flask of CHO-K1 (RRID: CVCL-0214) cells was from the Chinese Academy of Sciences Shanghai Institute of Life Sciences. Parental and plasmid-transfected CHO-K1 cells were routinely cultured in mixed medium DMEM/F12 (1:1), with further supplementation of fetal bovine serum (FBS, Gibco, Shanghai, China) at 10%, but without antibiotics, in a humidified CO_2 incubator (5% CO_2/95% air, 37°C).

The human thyroid follicular epithelial cell line SW579 (#1101HUM-PUMC000264) was from Cell Resource Center, Peking Union Medical College (http://cellresource.cn, Beijing, China). SW579 cells were cultured in Leibovitz's L-15 medium supplemented with 10% fetal bovine serum, in a humidified CO_2 incubator (closed environment with tightened flask caps, 37°C).

2.3 | Plasmid constructs

The *miniSOG* (JX999997) gene was synthesized (Genscript, Nanjing, China): ATGGAAAAGAGCTTTGTGATTACCGATC CGCGCCTGCCAGACAACCCGATCATTTTCGCGAGCGATG GCTTTCTGGAGTTAACCGAATATTCTCGTGAGGAAATTC TGGGTCGCAATGGCCGTTTCTTGCAGGGTCCGGAAACGG ATCAAGCCACCGTGCAGAAAATCCGCGATGCGATTCGTG ACCAACGCGAAATCACCGTTCAGCTGATTAACTATACGA AAAGCGGCAAGAAATTTTGGAACTTACTGCATCTGCAACC GATGCGCGATCAGAAAGGCGAATTGCAATATTTCATTGG TGTGCAGCTGGATGGCTAG. This *miniSOG* gene sequence was used to replace the *KillerRed* gene sequence in plasmid *pKillerRed*$_{PM}$, to obtain plasmid *pminiSOG*$_{PM}$. The *miniSOG* sequence in plasmid *pminiSOG*$_{PM}$ was amplified, cloned, and ligated to the 5′ end of the *NOX5* gene in *pcDNA*$^{3.1+}$ (RRID: Addgene-161738)*/NOX5*, to obtain plasmid *pminiSOG-NOX5* (RRID: SCR.002891, Genscript, Nanjing, China).

The above plasmids (*pminiSOG*$_{PM}$, *pcDNA*$^{3.1+}$*/NOX5*, *pminiSOG-NOX5*) and *pCMV3-DUOX2* were sequence verified. Each specific plasmid (2 μg DNA) was mixed well with transfection reagent (jetPRIME®, 4 μL) in a total transfection buffer volume of 200 μL, before addition to cell culture plate for transfection (200 μL of the complete mixture to one 35 mm culture plate). Twenty-four hours after transfection, the transfected CHO-K1 cells were used for immunocytochemistry or calcium imaging.

2.4 | Immunocytochemistry

The CHO-K1, NOX5-CHO-K1, miniSOG-NOX5-CHO-K1, SW579, and DUOX2-CHO-K1 cells grown on cover-slips were fixed (paraformaldehyde 4%, 10 min), before permeabilization (0.2% Triton X-100, 15 min). Nonspecific binding was blocked by bovine serum albumin (BSA 3%, 1 h). The processed cells on cover slips were first incubated with primary antibody (1:150, overnight at 4°C), before incubation with secondary antibody (30 min). All washes in between each step were performed in phosphate-buffered saline (PBS) with 0.2% Triton X-100 and 2% Tween-20. After the final wash, each

cell-attached cover slip was placed on a glass slide and stored at 4°C. Confocal imaging was done in a Zeiss LSM 510 META or Zeiss LSM 710 (Oberkochen, Germany), under objective 63/1.40 oil.

miniSOG was confocal imaged by its own fluorescence, $\lambda_{ex}/\lambda_{em}$ 488/501 nm; whereas nuclear DNA-binding dye 4′,6-diamidino-2-phenylindole (DAPI), $\lambda_{ex}/\lambda_{em}$ 405/495 nm. For immunocytochemistry, the primary antibodies, secondary antibodies and conjugated fluorophores, fluorophore excitation/emission wavelengths ($\lambda_{ex}/\lambda_{em}$), the Zeiss laser scanning confocal systems used are listed in Table 1.

2.5 | UVA light irradiation and photodynamic action

UVA irradiation of the NOX5-CHO-K1 cells was from a LED 380 nm (width at half height 10 nm) source (LAMPLIC, Shenzhen, China, http://www.szlamplic.com/), doses (380 nm, 0.1, 0.3, 3.5, 6, 12 mW/cm^2, 1.5 min) started from 0.1 mW/cm^2, based on previous work in RBL-2H3 (RRID: CVCL-0591) cells (380 nm, 80 μW/cm^2, 1.5 min).[22]

For SALPC photodynamic action, both SALPC concentration (2 μM) and light intensity (LED 675 nm, 85 mW/cm^2, 1.5 min) were referenced from previous works to photodynamically activate the cholecystokinin 1 receptor (red light from a halogen light source with a filter at >650 nm, 36.7 mW/cm^2, 2 min).[42–44] In the present work, the red light was from an LED 675 nm (width at half height 10 nm) source (LAMPLIC, Shenzhen, Guangdong, China, http://www.szlamplic.com/).

For miniSOG photodynamic action, the blue light was delivered at 85 mW/cm^2 for 1.5 min from a blue LED source 450 nm (width at half height 10 nm) (LAMPLIC, Shenzhen, China, http://www.szlamplic.com/); these parameters were similar to those used for miniSOG photodynamic activation of cholecystokinin 1 receptors (LED 450 nm, 85 mW/cm^2, 1.5 min).[45,46] All light intensities were measured with a power meter model IL-1700 (IL1715, Serial No. 3688, International Light Inc., Newburyport, MA, USA).

2.6 | Calcium imaging

Cytosolic calcium was measured in parental CHO-K1, or transfected NOX5-CHO-K1, miniSOG-NOX5-CHO-K1, SW579, and DUOX2-CHO-K1 cells by Fura-2 fluorescent imaging, as reported previously in other cells expressing the calcium-mobilizing cholecystokinin 1 receptor.[45–47] Briefly, Fura-2 AM (10 μM) was loaded into cells in a shaking water bath (37°C, 30 min). Fura-2-loaded cells were attached to Cell-Tak-coated cover-slip (with 1 μL of Cell-Tak 0.6 g/L smeared onto each cover-slip) at the bottom of a Sykes–Moore perfusion chamber, and perifused at 1 mL/min.[45–47] Alternatively, Matrix-gel was used at the same concentration as Cell-Tak. No difference was noted between Cell-Tak and Matrix-gel for cell adherence.

Calcium imaging was done in a Nikon NE 3000 fluorescence microscope, which was equipped with a Photon Technology International (PTI, now Horiba, Edison, NJ, USA) calcium measurement system. The intracellularly loaded Fura-2 was excited with excitation light from monochromator DeltaRam X, alternately at 340 and 380 nm (monochromater slit width 5 nm). The alternating (340/380 nm) excitation light intensity at the cell level was 0.370–1.092 μWatt/cm^2. Emitted fluorescent images were filtered at 510 ± 40 nm before capture on a NEO-5.5-CL-3 CCD (Oxford Instruments, Belfast, UK) (RRID: SCR.023609). Fluorescence intensity ratios of F_{340}/F_{380} were taken as indicative of intracellular calcium concentration. Fluorescent ratios of F_{340}/F_{380} were then plotted with Sigmaplot (RRID: 003210) against time, as reported before.[45–47]

2.7 | Data analysis

All data obtained, as integrated calcium peak areas above baseline (per 10 min), are presented as bar graphs showing means with 95% CI indicated. Data dots were superimposed on the bar columns. A paired two-tailed Student's *t*-test was done with Sigmaplot (RRID: 003210). For statistical analysis, a p value < 0.05 was taken as statistically significant, and marked with an asterisk (*).

TABLE 1 Immunocytochemical parameters.

Primary	Secondary	Fluorophore	$\lambda_{ex}/\lambda_{em}$ (nm)	LSM
Rabbit anti-NOX5	Donkey anti-rabbit	TRITC	543/573	510 Meta
Rabbit anti-DUOX2	Goat anti-rabbit IgG	Alexa Fluor® 488	488/563	710
Rabbit anti-DUOXA2	Goat anti-rabbit IgG	Alexa Flour® 568	561/640	710

Abbreviations: LSM, laser scanning microscope; TRITC, tetramethylrhodamine isothiocyanate.

3 | RESULTS

3.1 | UVA irradiation triggers calcium oscillations in NOX5-CHO-K1 cells

CHO-K1 cells were transfected in this work with plasmid *pcDNA*$^{3.1+}$*/NOX5*. Parental CHO-K1 cells were confirmed to express no endogenous NOX5 (Figure 1A, left), but 24 h after transfection with *pcDNA*$^{3.1+}$*/NOX5*, marked NOX5 expression was detected (Figure 1A, right). It was confirmed that when immunocytochemistry was performed in *pcDNA*$^{3.1+}$*/NOX5*-transfected CHO-K1 cells with the primary antibody omitted but with the secondary antibody present, no fluorescence was detected (data not shown). In the transiently transfected NOX5-CHO-K1 cells, NOX5 was found to be located at the plasma membrane and cytosol (red, Figure 1A, right, transfection rate was 34.7% ± 0.09%, calculated out of 3 independent experiments).

UVA irradiation (380 nm, 3.5 mW/cm^2, 1.5 min) (i.e., 315 mJ/cm^2) had no effect in parental CHO-K1 cells (Figure 1B) or in CHO-K1 cells transfected with the empty vector *pcDNA3.1*$^+$ (Figure 1C). The NOX5-CHO-K1 cell also presented a flat baseline in cytosolic calcium concentration without UVA light irradiation (Figure 1D). UVA (380 nm) light irradiation at power densities of 0.1, 0.3, 3.5, 6, and 12 mW/cm^2 (1.5 min) (i.e., 9, 27, 315, 540, 1080 mJ/cm^2), however, elicited conspicuous Ca^{2+} spikes in NOX5-CHO-K1 cells (Figure 1E–I), with very clear dose–response relationship (Figure 1J).

3.2 | UVA irradiation-induced calcium oscillations are inhibited by NOX inhibitor DPI and blocked by singlet oxygen quencher Trolox-C

In parallel experiments, it was found that the basal calcium concentration remained flat in NOX5-CHO-K1 cells in the dark (Figure 2A), but light (LED 380) at an intermediate dose of 3.5 mW/cm^2 (1.5 min) elicited robust calcium oscillations (Figure 2B). The perifusion of NOX inhibitor DPI 10 μM alone had no effect on basal calcium (Figure 2C), but after treatment with DPI 10 μM, UVA light irradiation (LED 380, 3.5 mW/cm^2, 1.5 min) no longer triggered any calcium oscillations (Figure 2D). The singlet oxygen quencher Trolox-C 300 μM had no effect on basal calcium concentration in NOX-5-CHO-K1 cells (Figure 2E), but could block completely the calcium spikes induced by UVA irradiation (LED 380, 3.5 mW/cm^2, 1.5 min) (Figure 2F). Statistical analysis of the calcium peak area above baseline showed that the effect of both DPI and Trolox-C was statistically significant (Figure 2G). These data suggest that UVA irradiation activated NOX5, possibly by $^1O_2$ generated in a UVA-driven type II photodynamic action.

3.3 | Photodynamic activation of NOX5 with photosensitizer SALPC

In this series of experiments, it was found that after perifusion of photosensitizer SALPC 2 μM, red light (675 nm, 85 mW/cm^2, 1.5 min) (i.e., 7.65 J/cm^2) irradiation elicited no effect in parental CHO-K1 cells (Figure 3A), which expressed no endogenous NOX5 as shown above in Figure 1A. Neither NOX5-CHO-K1 cells in the dark (Figure 3B), nor perfusion of SALPC 2 μM without subsequent light irradiation (Figure 3C), nor red light (675 nm, 85 mW/cm^2, 1.5 min) irradiation alone without SALPC exposure (Figure 3D) elicited any change in baseline calcium concentration in NOX5-CHO-K1 cells. However, when red light (675 nm, 85 mW/cm^2, 1.5 min) was applied after exposure to photosensitizer SALPC 2 μM, persistent cytosolic Ca^{2+} oscillation appeared in NOX5-CHO-K1 cell (Figure 3E). Such persistent calcium oscillation did not appear after photodynamic action (SALPC 2 μM, 675 nm, 85 mW/cm^2, 1.5 min) when NOX5-CHO-K1 cells were preincubated with the irreversible NOX inhibitor DPI 30 μM (Figure 3F). Analysis of calcium peak areas above baseline confirmed that DPI inhibition was statistically significant (Figure 3G). These data suggest that SALPC photodynamic action activated NOX5 in NOX5-CHO-K1 to elicit persistent Ca^{2+} oscillation.

3.4 | Photodynamic NOX5 activation with protein photosensitizer miniSOG

To investigate the possible photodynamic action of protein photosensitizer miniSOG on NOX5, we made a fusion construct of miniSOG-NOX5 (Figure 4A), with the *miniSOG* gene ligated to the 5′ end of the *NOX5* gene in *pcDNA3.1*$^+$*/NOX5*. Plasmid *pminiSOG-NOX5* was used to transfect CHO-K1 cells; expression of fusion protein miniSOG-NOX5 was detected by immunocytochemistry. Plasma membrane and cytoplasmic co-localization of miniSOG and NOX5 was confirmed in the miniSOG-NOX5-CHO-K1 cells (Figure 4B, transfection rate 21.6% ± 0.50%, calculated out of 3 independent experiments).

Blue LED light (450 nm, 85 mW/cm^2, 1.5 min) (i.e., 7.65 J/cm^2) irradiation had no effect on NOX5-CHO-K1 cells (Figure 4C). Therefore with no co-expressed miniSOG, blue light showed no effect on NOX5 in NOX5-CHO-K1 cells—the cytosolic calcium remained flat at

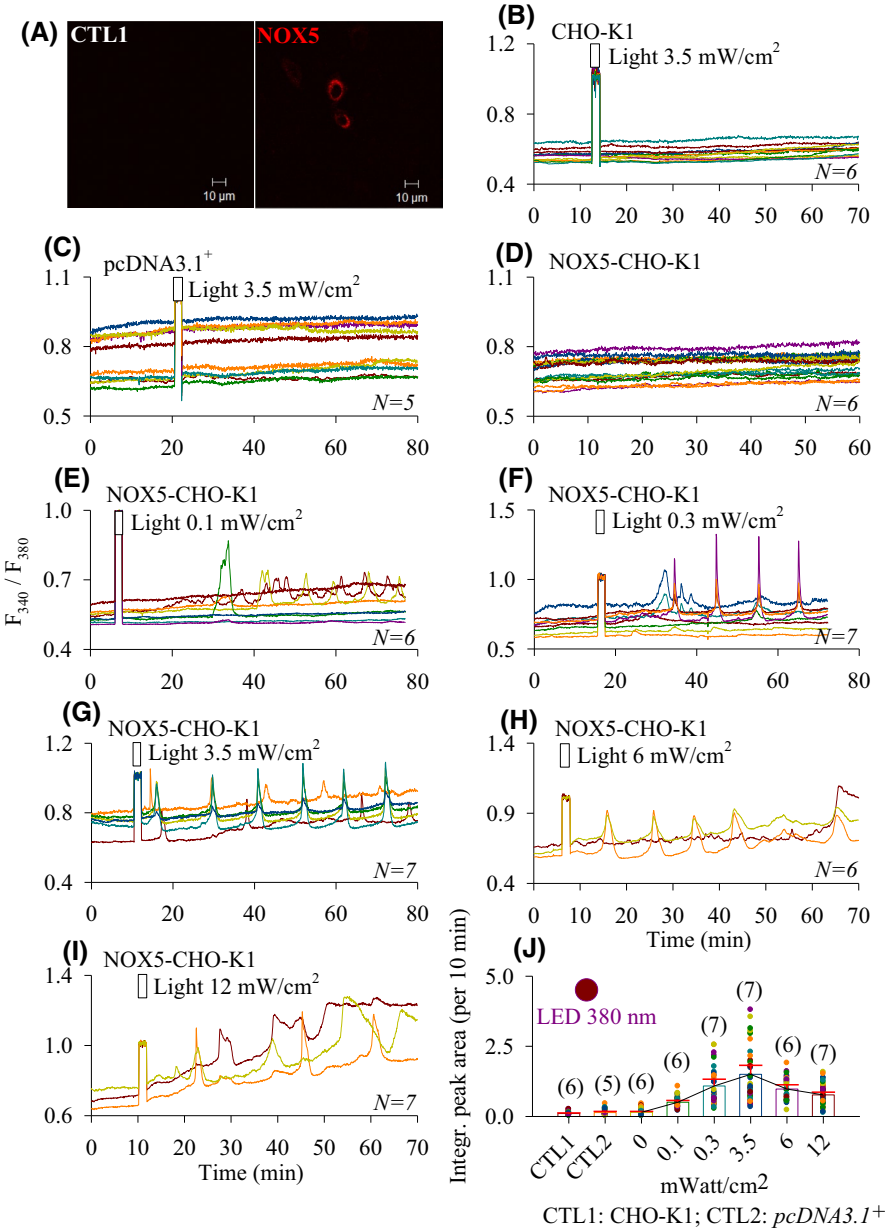

CTL1: CHO-K1; CTL2: *pcDNA3.1*$^+$

FIGURE 1 UVA irradiation triggered calcium oscillations in NOX5-CHO-K1 cells. (A) The *pNOX5*-transfected CHO-K1 cells were fixed for NOX5 immunocytochemistry. Note the bright fluorescence in transfected NOX5-CHO-K1 cells (A, right), but no fluorescence in un-transfected parental CHO-K1 cells (A, left) (CTL1, control). Scale bar: 10 μm. (B–I) Fura-2-loaded cells were perifused for calcium imaging: (B) CHO-K1 (CTL1); (C) empty vector (*pcDNA3.1*$^+$) transfected CHO-K1 cells (CTL2); or (D–I) NOX5-CHO-K1 cells. These cells were either perifused in the dark (D), or exposed to UVA light at indicated power density (LED 380 nm, 0.1, 0.3, 3.5, 6, 12 mW/cm^2, 1.5 min) (B, C, E–I), as indicated by the horizontal bars. The calcium tracings (each trace corresponds to one individual cell) shown in each panel (B–I) are from one typical experiment, out of *N* identical ones ($N = 5$–7). (J) The dose–response relationship for UVA irradiation-induced calcium spikes (area under the curve above baseline, per 10 min), the *N* numbers are indicated in brackets above each column. Bar graphs showing means with 95% CI indicated. Each data dot on the bar column represents one cell.

the baseline level (Figure 4C). Basal calcium was stable also without light irradiation in miniSOG-NOX5-CHO-K1 cells (Figure 4D). However, after blue LED-light (450 nm, 85 mW/cm^2, 1.5 min) irradiation, persistent Ca^{2+} oscillation emerged in miniSOG-CCK2R-CHO-K1 cells (Figure 4E). The NOX inhibitor DPI alone had no effect on basal calcium in miniSOG-CCK2R-CHO-K1 cells (Figure 4F), but previous incubation with DPI 10 μM blocked completely the blue LED light-triggered Ca^{2+} oscillation (Figure 4G). Calculation of calcium peak areas revealed that NOX inhibitor DPI effect was statistically significant (Figure 3H). These data suggest that photodynamic action with the in-frame miniSOG photodynamically activated NOX5 in miniSOG-NOX5, to trigger calcium oscillation in miniSOG-NOX5-CHO-K1 cells.

In time-matched (i.e., done on the same day with the same batch of transfected cells) parallel control experiments, it was found that Trolox-C 300 μM had no effect on baseline calcium concentration in miniSOG-NOX5-CHO-K1 cells (Figure 4I). Blue LED light (450 nm, 85 mW/cm^2, 2 min) irradiation elicited conspicuous Ca^{2+} spikes in miniSOG-NOX5-CHO-K1 cells (Figure 4J). In contrast, when Trolox-C 300 μM (a dose known to block miniSOG photodynamic activation of cholecystokinin 1 receptors), see Refs.[45,46] was added to the perfusion buffer, blue LED light no longer induced any calcium spikes in miniSOG-NOX5-CHO-K1 cells (Figure 4K). A comparison of integrated calcium peak area indicated that Trolox-C 300 μM inhibited significantly calcium response triggered by LED blue light irradiation (Figure 4L, $p < 0.05$). These data suggest that photodynamic action with in-frame miniSOG

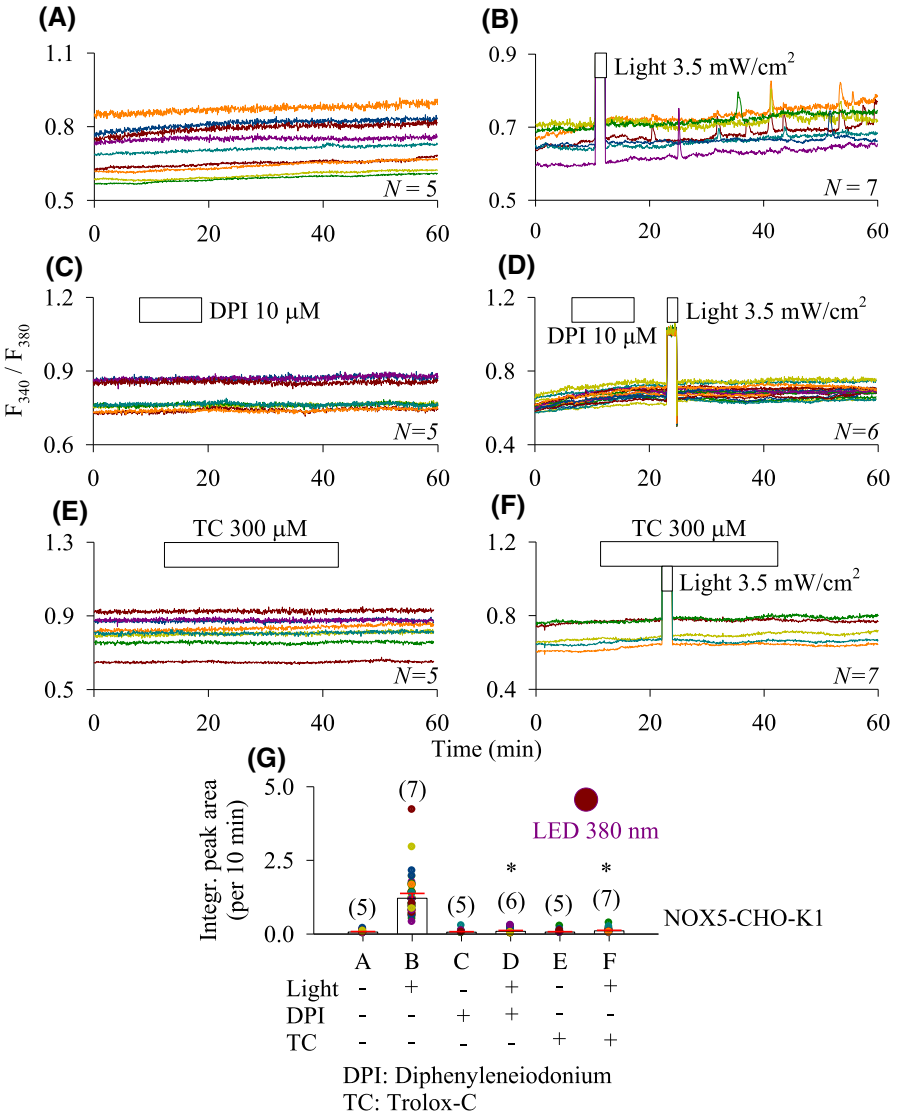

FIGURE 2 UVA irradiation-induced calcium oscillations are inhibited by NOX inhibitor DPI and blocked by $^1O_2$ quencher Trolox-C. (A–F) Fura-2 AM-loaded NOX5-CHO-K1 cells were perifused in the dark alone (A), or exposed to UVA irradiation (380 nm, 3.5 mWatt/cm^2, 1.5 min) (B, D, F); DPI 10 µM (C, D) or Trolox-C 300 µM (E, F) were added as indicated by the horizontal bars. Calcium tracings (each trace corresponds to one cell) shown in each panel (A–F) are from one typical experiment, out of *N* identical ones (*N* = 5–7). (G) Bar graphs showing means with 95% CI indicated. Quantitative analysis of calcium peak areas above baseline (per 10 min) from multiple experiments (*N* = 5–7). The *N* numbers are shown in brackets above each column, with each dot representing data from one cell. Student's *t* test was used for comparison between light alone (B) with light + DPI (D) or with light + TC (F). *Asterisk indicates $p < 0.05$.

activated the in-frame NOX5, likely via $^1O_2$ as the reactive intermediate.

Other than NOX2 Ref.[21,22] and NOX5 (Figures 1–4, present work), DUOX2 was activated similarly by UVA irradiation and photodynamic action, as shown below in Section 3.5.

3.5 | UVA irradiation triggers calcium oscillation in thyroid follicular cells SW579

Immunocytochemistry with confocal imaging confirmed that DUOX2 was present in the plasma membrane and cytosol in SW579 cells (Figure 5B) but no fluorescence was seen in the absence of the primary antibody (Figure 5A). Perifused resting SW579 cells showed a stable basal calcium level (Figure 5C). A very short UVA (380 nm, 0.1 mWatt/cm^2) pulse of 1 s had no effect on the baseline calcium (Figure 5D) in SW579 cells, but longer pulses of 10, 30, 60, and 90 s all induced robust calcium spikes, dose dependently (Figure 5E–H). Pretreatment with NOX inhibitors DPI (10 µM, 10 min) or VAS2870 (20 µM, for 30 min before time 0) was able to inhibit completely the calcium oscillations induced with UVA 90 s in SW579 cells (Figure 5I,J), as treatment with $^1O_2$ quencher Trolox-C (300 µM) (Figure 5K). Quantification of the calcium peak areas above baseline (per 10 min) after UVA exposure indicated a clear dose–response relationship for UVA irradiation (0, 1, 10, 60, 90 s), and statistically significant inhibition of the effect of UVA pulse (90 s) with DPI (10 µM), VAS2870 (20 µM), and Trolox-C (300 µM) (Figure 5L).

3.6 | UVA irradiation and SALPC photodynamic action trigger calcium oscillations in DUOX2-CHO-K1 cells

The parental CHO-K1 cells did not show significant expression of DUOX2 (Figure 6A), but did show endogenous expression of DUOXA2 (see Figure 6A′B′), strong DUOX2

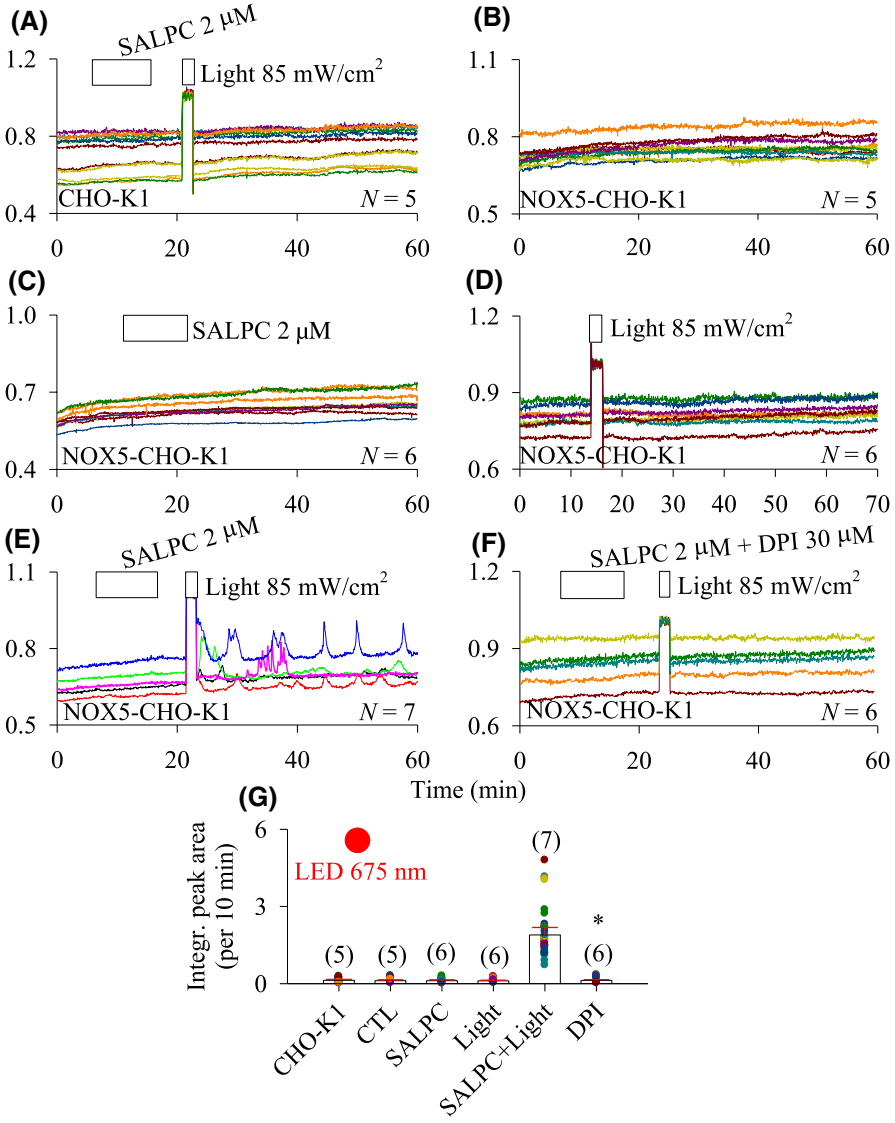

FIGURE 3 Photodynamic activation of NOX5 with photosensitizer SALPC. (A–F) Fura-2-loaded CHO-K1 (A), NOX5-CHO-K1 (B–F) cells were perifused, SALPC 2 μM (A, C, E, F), red light (LED 675 nm, 85 mW/cm^2, 1.5 min) (A, D, E, F) or DPI 30 μM (F) were applied as indicated by the horizontal bars. (A–F) Calcium tracings (each trace corresponds to one individual cell) shown in each panel (A–F) are from one typical experiment, out of *N* repeats ($N = 5–7$). (G) Bar graphs showing means with 95% CI indicated. The integrated calcium peak areas above baseline (per 10 min) were compared among the different experiments shown in (A–F) ($N = 5–7$), with each dot representing data from one cell. Student's *t* test was used for comparison between SALPC + Light without (E) or with DPI (F). Asterisk (*) indicates statistical significance at $p < .05$.

expression was noted in DUOX2-CHO-K1 cells (Figure 6B). Perifused CHO-K1 cells did not respond to UVA irradiation (Figure 6C), DUOX2-CHO-K1 cells in the dark similarly showed flat baseline calcium (Figure 6D). A pulse of UVA (380 nm, 3.5 mWatt/cm^2, 1.5 min) elicited robust calcium oscillations in DUOX2-CHO-K1 cells (Figure 6E). The NOX inhibitor VAS2870 (3 μM) had no effect on baseline calcium (Figure 6F), but could suppress completely calcium spikes elicited by UVA (Figure 6G). Photodynamic action with SALPC (675 nm, 85 mWatt/cm^2, 90 s) had no effect in un-transfected CHO-K1 cells (Figure 6H), as SALPC alone in the dark in DUOX2-CHO-K1 cells (Figure 6I), or light alone in the absence of previous incubation with SALPC in DUOX2-CHO-K1 cells (Figure 6J). Photodynamic action with SALPC (red LED 675 nm), however, trigged persistent calcium spikes, a hallmark of permanent photodynamic activation of DUOX2 (Figure 6K). Quantification of the calcium peak area above baseline (per 10 min) showed the statistical data from the above experiments performed multiple times (Figure 6L).

4 | DISCUSSION

We have found here that the human NOX5 expressed ectopically in the rodent CHO-K1 cell line was activated dose dependently by a brief pulse of UVA light irradiation (1.5 min) to induce persistent calcium spikes. A brief pulse of photodynamic action (1.5 min) with photosensitizer SALPC or in-frame miniSOG, in NOX5-CHO-K1 or miniSOG-NOX5-CHO-K1 cells, respectively, similarly triggered persistent calcium oscillations. These calcium oscillations induced by UVA irradiation or photodynamic action were all inhibited by the pan-NOX inhibitor DPI and blocked with $^1O_2$ quencher Trolox-C. Similar effects of UVA irradiation and SALPC photodynamic action were observed in the human thyroid follicular cell line SW579 and in DUOX2-CHO-K1 cells. Therefore a short period (1.5 min) of both UVA irradiation and photodynamic action could activate NOX5 and DUOX2, likely via intermediate $^1O_2$, to ultimately trigger periodic calcium increases.

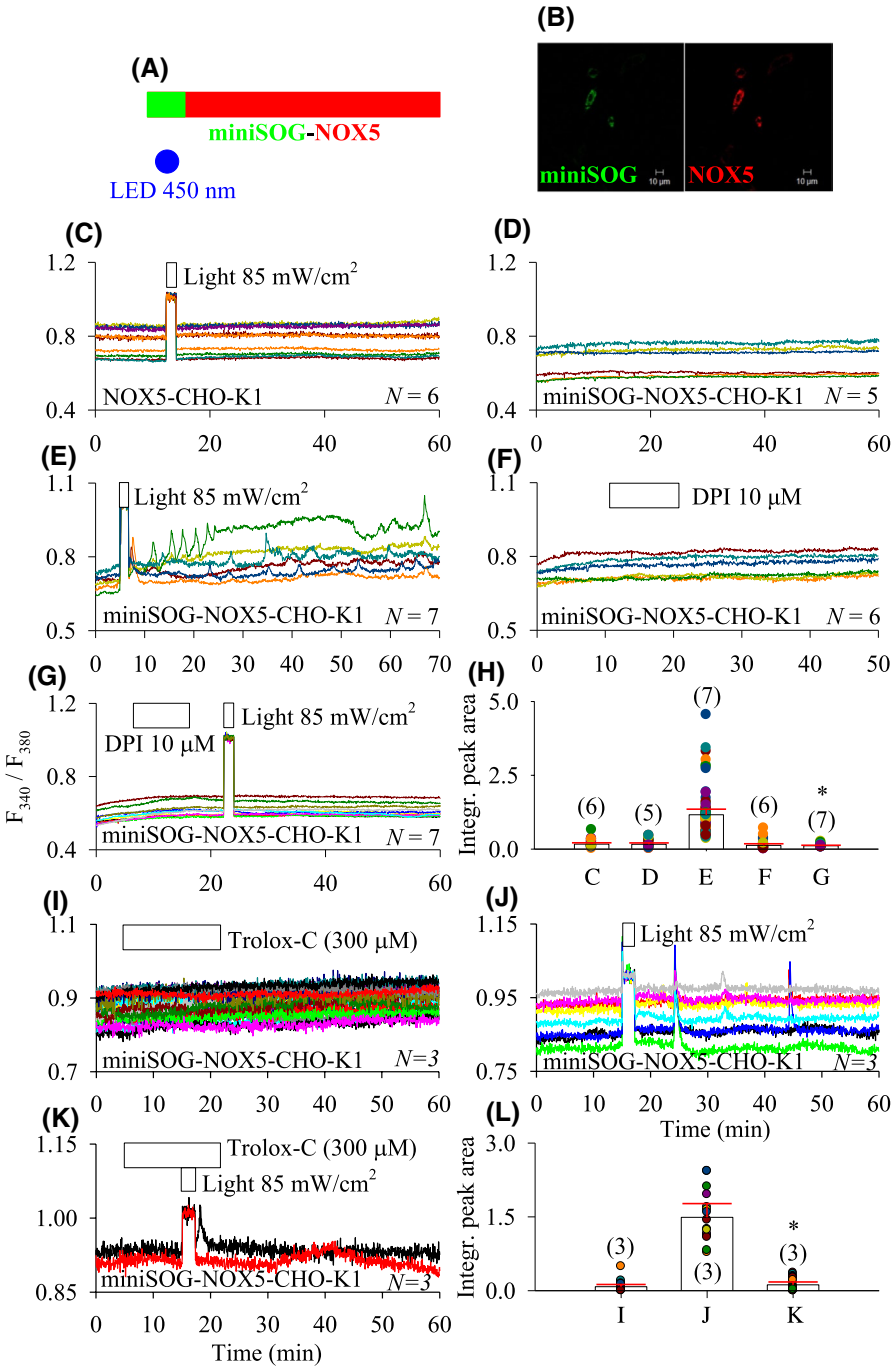

FIGURE 4 The miniSOG photodynamic activation of NOX5 with protein photosensitizer miniSOG. (A, B) Fusion gene for construct miniSOG-NOX5 was expressed in CHO-K1 cells, as confirmed by miniSOG-NOX5 immunocytochemistry. Scale bars: 10 μm. (C–G, I–K) Fura-2-loaded NOX5-CHO-K1 (C) or miniSOG-NOX5-CHO-K1 cells (D–G, I–K) were perifused, blue light (LED 450 nm, 85 mW/cm^2, 1.5 min) (C, E, G, J, K), DPI 10 μM (F, G) or Trolox-C 300 μM (I, K) were applied (indicated by horizontal bars). These calcium tracings (each trace corresponds to one individual cell) shown (C–G, I–K) are from one typical experiment each, out of *N* identical repeats (*N* = 3–7). (H, L) Bar graphs showing means with 95% CI indicated. Statistical data were calculated from *N* experiments, to compare calcium peak area above baseline (per 10 min), with *N* numbers shown on each column in (H, L). Each dot on the bar column represents data from one cell. Student's *t* test was used for statistical comparison, between Light (E) and Light + DPI (G) in panel (H), between Light (J) and Light + Trolox-C (K), the asterisk (*) indicates statistical significance at $p < 0.05$.

UVA irradiation was initially found to activate NAD(P)H oxidase (NOX) in rat peritoneal mast cell, to trigger persistent Ca^{2+} oscillation.[21] UVA triggered calcium oscillations in mast cells of at least three different sources (rat peritoneal mast cell, mouse bone marrow-derived mast cell, rat mast cell line RBL-2H3).[22] Knocked-down expression of NOX2, P22, or P47 in RBL-2H3 cells effectively inhibited calcium oscillation triggered by UVA irradiation.[22] UVA activation of NOX2 results in $O_2^{\cdot -}$ generation, to subsequently activate the signaling pathway of receptor tyrosine kinase–phospholipase Cγ–inositol 1,4,5-trisphosphate (IP_3)–IP_3 receptor (IP_3R)–Ca^{2+}, to trigger persistent Ca^{2+} oscillation.[21,22]

UVA light irradiation has also been shown previously to activate NOX1 in human keratinocytes[48] and to elicit P67 (a cytosolic subunit for NOX2) membrane translocation in the human acute monocytic leukemia cell line THP-1[49]; in these works the detection endpoint was production of reactive oxygen species.[48,49] NOX isozyme activation could also be gauged after cell lysis by phosphorylation of cytosolic subunit P47[50] or P67.[51] But this was a multistep process, unlike the single-step fluorescent measurement of cytosolic calcium or of reactive oxygen species. Since activation of the single subunit NOX5 does not involve any accessory subunits of P22,

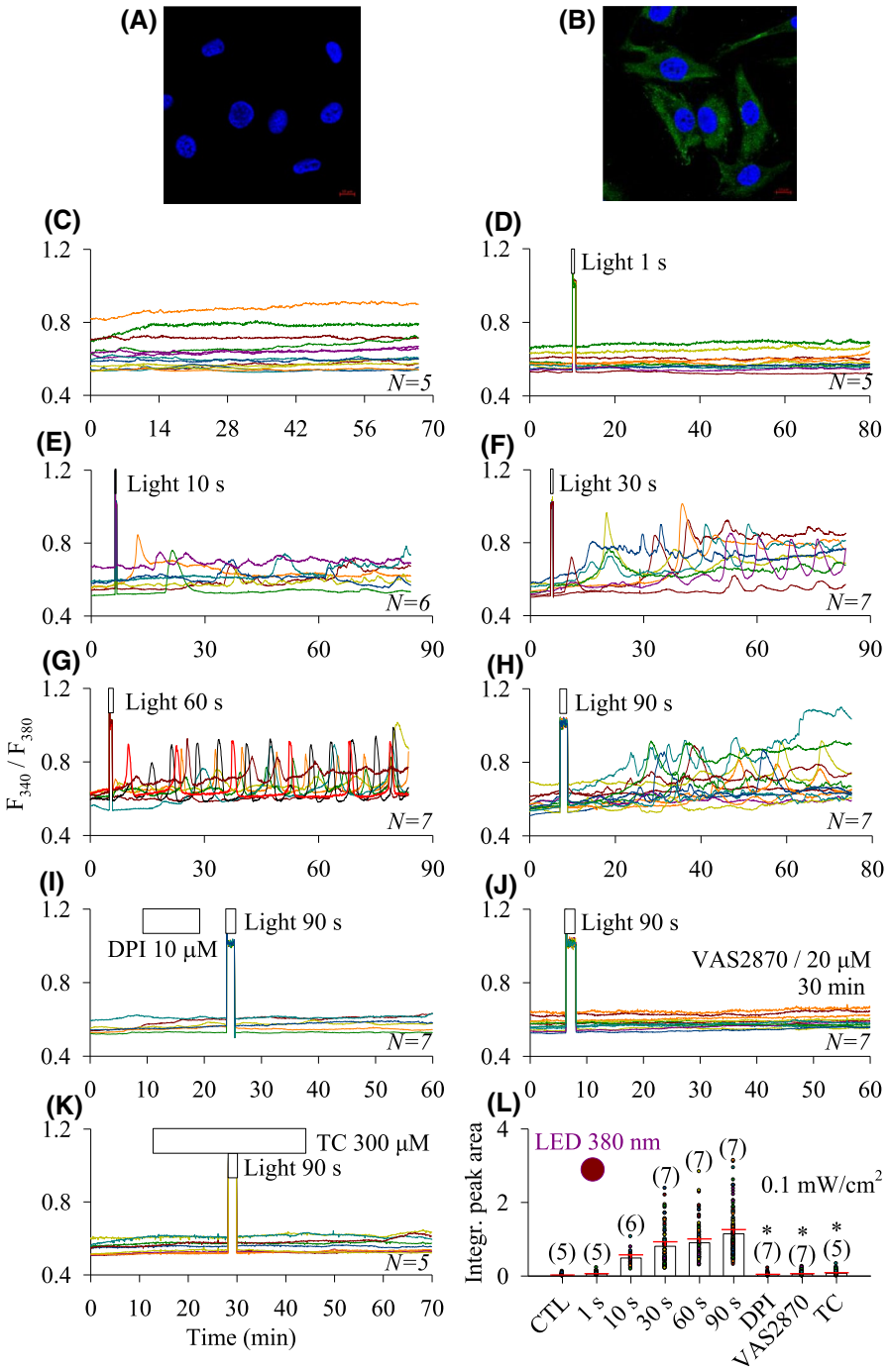

FIGURE 5 UVA irradiation triggered calcium oscillations in SW579 cells. (A, B) SW579 cells grown on cover-slips were fixed for DUOX2 immunocytochemistry. Note the strong fluorescence in cells incubated with primary and secondary antibodies (B), but no fluorescence in cells with primary antibody omitted (A). Scale bars 10 µm. (C–K) Fura-2 AM loaded SW579 cells were attached to cover-slips and perifused. The SW579 cells were either perifused in the dark (C), or exposed to UVA light (LED 380 nm, 0.1 mWatt/cm^2) for 1 (D), 10 (E), 30 (F), 60 (G), 90 s (H–K). UVA (380 nm, 0.1 mWatt/cm^2) (D-K), DPI (10 µM) (I), VAS2870 (20 µM, 30 min) (preincubated) (J), or Trolox-C (300 µM) (K), were applied as indicated by the horizontal bars. The typical calcium traces (each trace corresponds to one individual cell) shown in (C–K) are from one typical experiment, out of *N* identical repeats ($N = 5$–7) (L) Bar graphs showing means with 95% CI indicated are quantitative analysis of calcium peak areas above baseline (per 10 min) from multiple experiments (*N* numbers shown in brackets), each dot represent data from one cell. Student's *t* test was used for comparison between Light 90 s (H), and Light 90 s together with DPI (I), VAS2870 (J), or Trolox C (TC) (K). Asterisk (*) indicates statistical significance at $p < 0.05$.

P40, P47, P67, Rac1/2,[24,52] P47/P67 phosphorylation or their membrane transfer will not be indicative of NOX5 activation. In fact, it has been noted that with NOX2, phosphorylation of the catalytic subunit gp91^{phox}/NOX2 itself actually results in inhibited gp91^{phox}/NOX2 activity.[53]

In this work, we expressed the human NOX5 heterologously in the rodent CHO-K1 cells, an easy-to-transfect cell line with a competent calcium signaling pathway.[54] Immunocytochemistry confirmed NOX5 expression in the cytoplasma and on plasma membrane in NOX5-CHO-K1 cells (Figure 1), similar to NOX5 distribution in transfected COS-7 cells, cultured human endothelial cells or prostate cancer cells.[55–57] UVA (380 nm, 0.1, 0.3, 3.5, 6, 12 mW/cm^2, 1.5 min) was found to trigger dose dependently calcium transients in the NOX5-CHO-K1 cell, but the high dose of 3.5 mW/cm^2 showed no effect in the parental cell CHO-K1 or empty vector-transfected pcDNA3.1$^+$-CHO-K1 cells (Figure 1), or in HEK293 cells (data not shown).

UVA irradiation-induced calcium oscillations were inhibited completely by preincubation with the NOX inhibitor DPI 10 µM, and blocked by $^1O_2$ quencher Trplox-C (Figure 2). DPI inhibits NOX by binding to the "flavin and heme prosthetic groups to form stable adducts",[58] therefore

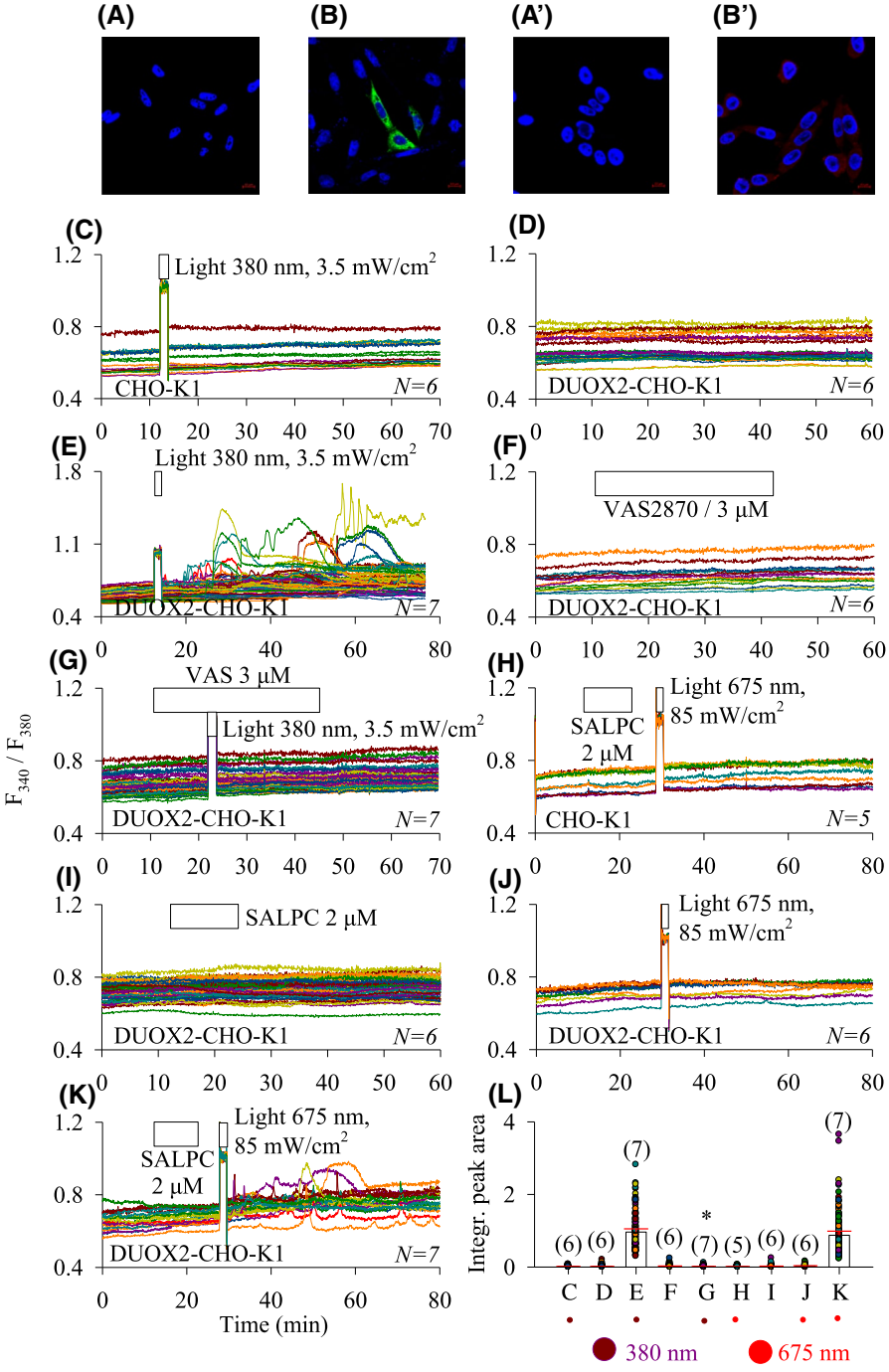

FIGURE 6 UVA irradiation and SALPC photodynamic action triggered calcium oscillations in DUOX2-CHO-K1 cells. (A, A′, B′) Parental CHO-K1 cells. (B) DUOX2-CHO-K1 cells. Cells were fixed for DUOX2 (A, B) or DUOXA2 (A′, B′) immunocytochemistry. No DUOX2 fluorescence was detected in un-transfected parental cells CHO-K1 (A), but note the strong DUOX2 fluorescence in transfected DUOX2-CHO-K1 cells (B). DUOXA2 was noted in parental CHO-K1 cells (compare A′, B′), primary antibody was omitted from (A′). Scale bars 10 µm. (C–K) Fura-2 AM-loaded CHO-K1 (C, H), DUOX2-CHO-K1 cells (D–G, I–K) were perifused, UVA (380 nm, 3.5 mWatt/cm^2, 1.5 min) (C, E, G), VAS2870 (3 µM) (F, G), SALPC 2 µM (H, I, K), red LED (675 nm, 85 mWatt/cm^2, 1.5 min) (H, J, K) were applied as indicated by the horizontal bars. Original calcium tracings (each trace corresponds to one individual cell) shown in panels C-K are each from one typical experiment, out of *N* identical repeats ($N = 5–7$). (L) Bar graphs showing means with 95% CI indicated are quantitative analysis of calcium peak areas above baseline (per 10 min) from multiple experiments (*N* number are shown in brackets, each dot on column represents data from one cell). Student's *t* test was used for comparison between Light (E) and Light + VAS2870 (G), asterisk (*) indicates statistical significance at $p < 0.05$.

DPI could be used by preincubation. These data suggest that UVA irradiation, likely via type II photodynamic action (i.e., via $^1O_2$), activated NOX5 to trigger persistent calcium oscillations. $^1O_2$ activation of NOX5 likely triggers the same electron transfer process of NADPH–FAD–heme–O_2 to produce $O_2^{\cdot-}$ as other stimuli.[24] $O_2^{\cdot-}$ so produced would then activate the receptor tyrosine kinase–phospholipase Cγ–IP_3–IP_3R–Ca^{2+} signaling pathway, to elicit increases in cytosolic calcium concentration, same as UVA-driven NOX2 activation-induced persistent calcium oscillations in mast cells.[21,22,59] Unlike with the multi-subunit $gp97^{Phox}$-NOX2 (NOX2 + P22 + P40 + P47 + P67 + Rac), with the single catalytic subunit only NOX5, it can be concluded that UVA activation of NOX5 must be due to absorption of UVA (LED 380 nm) photons by NOX5.

It is known that UVA absorption by unbound free endogenous photosensitizers NAD(P)H and FAD elicits type II photodynamic action to produce $^1O_2$, with a quantum yield ($\Phi\Delta^1O_2$) of ≥0.1 and 0.07, respectively.[27,29] The coordinately bound NAD(P)H and FAD in the C-terminal dehydrogenase domain of NOX5 after absorption of UVA photons (LED 380 nm) may also undergo similar, although likely somewhat damped, photodynamic action due to protein caging, to generate $^1O_2$ within the NOX5 protein molecule, which in turn may facilitate the transformation of the resting NOX5 to the activated state. To verify whether photodynamic action is involved in UVA activation of NOX5, photodynamic action with photosensitizer SALPC, with a ΦΔ of 0.38,[37,38] was used. Note that brief incubation with SALPC has been used before for plasma membrane-localized type II photodynamic action, to activate the cholecystokinin 1 receptor.[42–44,60]

Indeed SALPC photodynamic action (675 nm, 85 mW/cm^2, 1.5 min) readily triggered persistent cytosolic Ca^{2+} oscillation in the NOX5-CHO-K1 cells (Figure 3), which was inhibited completely by pretreatment with NOX5 inhibitor DPI 30 μM (Figure 3). Time-matched control experiments showed that SALPC photodynamic effect did not affect basal calcium in parental CHO-K1 cells which expressed no endogenous NOX5 (Figure 3). Neither SAPLC alone nor light irradiation alone without preincubation with SALPC had any effect on baseline calcium concentration in NOX5-CHO-K1 cells (Figure 3). Therefore SALPC photodynamic action at the plasma membrane activated NOX5, to trigger persistent calcium oscillations.

Photodynamic action with the protein photosensitizer miniSOG was found to have a similar effect. The miniSOG after absorbing blue light (LED 450 nm) produces $^1O_2$ at a ΦΔ of ≥0.03.[41,61] $^1O_2$ has a rather limited lifetime (1 μs) therefore a limited diffusion distance (10–155 nm).[35,62,63] Tagging miniSOG to NOX5 would ensure spatially delimited photodynamic action, probably around the expressed miniSOG-NOX5 construct. Photodynamic action (450 nm, 85 mW/cm^2, 1.5 min) with the in-frame miniSOG of construct miniSOG-NOX5 was found to similarly elicit persistent Ca^{2+} oscillations, which were inhibited completely by pretreatment with DPI 10 μM, and blocked completely by $^1O_2$ quencher Trolox-C (Figure 4). These data indicate that miniSOG photodynamic action activated NOX5 in miniSOG-NOX5-CHO-K1 cells, likely via the reactive intermediate of $^1O_2$ (Figure 4).

Data obtained in this work (Figures 1–4) therefore confirm that NOX5 could be activated by a brief pulse of photodynamic action, executed either with UVA irradiation (1.5 min) (via NOX5-bound endogenous photosensitizers) or with blue or red LED irradiation (1.5 min) with exogenous photosensitizer SALPC or in-frame miniSOG, respectively. During this photodynamic process, the light sources used were UVA LED 380 nm (Figures 1 and 2), blue LED 450 nm (Figure 4), and red LED 675 nm (Figure 3).

NOX5, same as the catalytic subunit of all other NOX isozymes, coordinately binds NADPH, FAD, and two heme molecules, the absorption spectra of these molecules when dissolved free in solvent are shown in Figure S1. UVA 380 nm is absorbed by all three chromophores, blue 450 nm by FAD and heme, but red 675 nm is not absorbed by any of them, as reported in the literature[29,64–67] (Figure S1). However, only UVA 380 nm (0.1–12 mWatt/cm^2) alone effectively activated NOX5 (Figures 1E–I and 2B), but red LED 675 nm alone (85 mWatt/cm2) (Figure 3D) or blue LED 450 nm alone (85 mWatt/cm2) (Figure 4C) in the absence of SALPC or miniSOG did not (Figures 3D and 4C).

Of the three NOX5 chromophores of NAD(P)H, FAD, heme, only FAD and NADPH are effective photosensitizers, with quantum yield ($\Phi\Delta^1O_2$) of FAD 0.07 and NADPH ≥0.1.[41,61] The absorption extinction coefficient at 380 nm is, FAD 8 $mM^{-1}cm^{-1}$, NADPH 1 $mM^{-1}cm^{-1}$.[65,66] Note that for FAD, absorption peak at 450 nm is larger than at 375 nm, whereas NADPH shows no absorption beyond 400 nm (Figure S1), as noted previously in the literature.[65,66] This may indicate that NADPH alone or NADPH and FAD in combination or simultaneously are the responsible photosensitizer(s) to mediate UVA irradiation-powered photodynamic activation of NOX5.

Other than NOX5 (Figures 1–4, present work) and NOX2,[21,22] it was found in the present work that the native human DUOX2 in thyroid follicular epithelial cell line SW579 and in DUOX2-CHO-K1 was also activated by UVA irradiation (Figures 5 and 6). UVA irradiation triggered calcium oscillations dose dependently, and such oscillations were inhibited by NOX inhibitors (DPI and VAS2870) and blocked with $^1O_2$ quencher Trolox-C (Figure 5). Although CHO-K1 cells expressed endogenous DUOXA2 (G3H0S2), endogenous DUOX2 seemed rather low or undetectible; UVA irradiation had no effect on basal calcium in CHO-K1 cells (Figure 6). After plasmid transfection the DUOX2

expression was markedly increased in DUOX2–CHO-K1 cells (Figure 6). The presence of endogenous DUOXA2 expression may account for the fact that DUOX2–CHO-K1 cells showed a ready response to UVA irradiation and SALPC photodynamic action since it is known that the full functionality of DUOX2 requires the presence of DUOXA2.[68] Human DUOX2 ectopically expressed in rodent CHO-K1 cells was activated by UVA irradiation and SALPC photodynamic action (Figure 6). UVA irradiation-induced calcium oscillations were completely blocked by the NOX inhibitor VAS2870 (3 μM) (Figure 6). Further, SALPC photodynamic action triggered persistent calcium oscillations in DUOX2-CHO-K1 cells (Figure 6), similar to those observed in NOX5-CHO-K1 cells (Figure 3). Note that the human thyroid follicular epithelial tumor cell SW579 was very sensitive to UVA irradiation; a 10 sec LED 380 pulse at 0.1 mWatt/cm^2 was sufficient to trigger detectable calcium oscillations, a rather low dose similar to that used in primary rodent mast cells or mast cell line.[22] Even for this very sensitive cell type of SW579, the alternating excitation light (power density: ≦1.092 μWatt/cm^2, from the monochrometer DeltaRam X) for Fura-2 fluorescence calcium imaging, did not seem to interfere with calcium measurement; basal calcium remained completely flat without extra LED 380 nm irradiation (Figure 5C).

$^1O_2$ at low concentrations is a signaling molecule in multiple cell types[35,69–71] but at higher concentrations are cytocidal therefore is used for photodynamic therapy (PDT) of both benign and cancerous lesions.[72,73] $^1O_2$ susceptible residues (Met, Cys, His, Trp, Tyr) are abundant in NOX5, concentrated particularly in the FAD-binding domain (Y^{441}, $H^{444,461}$, $W^{443,459,468}$) and near the NADPH-binding domain ($M^{558}Y^{559}$, $H^{627}M^{628}Y^{629}M^{630}$) in the C-terminal cytosolic dehydrogenase region (Figure S2).[74] Interestingly, the Cys-containing motif of ^{369}Cys-Gly-Cys^{371} in the catalytic NOX2 and Cys residues in P67^{Phox} have been found to be important for NOX2-P67 binding/association and NOX2 activation induced by oxidants.[75,76]

NOX5 is known to regulate cell growth, differentiation, and migration.[25] Excessive ROS production by NOX5 is associated with coronary atherosclerosis,[77] acute myocardial infarction,[78] fetal ventricular septal defect,[79] or cancer.[80] $O_2^{\cdot-}$-related diseases could be due to either complete loss of $O_2^{\cdot-}$ generation or overproduction of $O_2^{\cdot-}$.[81] DUOX2 as well, is involved in vital physiological functions. DUOX2 is predominantly expressed in the thyroid follicular epithelial cells for thyroid hormone synthesis,[82] and in the gastrointestinal and respiratory epithelial cells probably for innate immunity.[83,84] The present work provides a novel method to experimentally activate NOX5 and DUOX2 for localized production of $O_2^{\cdot-}/H_2O_2$. Since data from the present work suggest that the catalytic subunit-only NOX5 alone is activated by a brief pulse of UVA irradiation/photodynamic action (1.5 min), NOX isoforms other than NOX2,[21,22] NOX5, and DUOX2 (present work) may be similarly activated. Focused light-driven permanent photodynamic NOX isozyme activation will provide a useful means for the study of NOX1-5 and DUOX1,2 physiology, pathophysiology, and related therapeutics.[85,86]

The current understanding of the structural biology and chemistry[23,87–91] of NADPH oxidases and their activation, together with what we have found in the present work, will provide a solid background for further investigation and the detailed elucidation of photodynamic activation of NOX family members of NOX1-5 and DUOX1,2. Specifically, cellular works with mutated NOX5, together with biochemical works with purified NOX5 or DUOX2 proteins, and cryoEM studies of such enzymes with tagged protein photosensitzers (such as miniSOG) in the future, will reveal the detailed mechanisms of UVA and photodynamic activation of NOX enzymes.

AUTHOR CONTRIBUTIONS

Zong Jie Cui conceived the idea of this study. Xiao Bing Xie and Yu Shu performed the experiments, analyzed the data, and wrote initial drafts of the MS. Zong Jie Cui acquired funding for this work and supervised the experimentations and data analysis. Zong Jie Cui finalized the submitted version of the MS. All authors (Xiao Bing Xie, Yu Shu, Zong Jie Cui) approved the submission of this MS.

ACKNOWLEDGMENTS

This work was supported by a grant from The Natural Science Foundation of China (NSFC, grant No. 32271278).

DISCLOSURES

The authors declare no conflicts of interest.

DATA AVAILABILITY STATEMENT

All data are contained in this paper. Original data will be available upon reasonable request to the corresponding author.

ORCID

Xiao Bing Xie https://orcid.org/0009-0009-1921-6614
Zong Jie Cui https://orcid.org/0000-0003-4252-4876

REFERENCES

1. Chandel NS. NADPH—the forgotten reducing equivalent. *Cold Spring Harb Perspect Biol*. 2021;13:a040550. doi:10.1101/cshperspect.a040550
2. Niu X, Stancliffe E, Gelman SJ, et al. Cytosolic and mitochondrial NADPH fluxes are independently regulated. *Nat Chem Biol*. 2023;19:837-845. doi:10.1038/s41589-023-01283-9
3. Bedard K, Krause KH. The NOX family of ROS-generating NADPH oxidases: physiology and pathophysiology. *Physiol Rev*. 2007;87:245-313. doi:10.1152/physrev.00044.2005

4. Brown DI, Griendling KK. NOX proteins in signal transduction. *Free Radic Biol Med*. 2009;47:1239-1253. doi:10.1016/j.freeradbiomed.2009.07.023
5. Nazari B, Jaquet V, Krause KH. NOX family NADPH oxidases in mammals: evolutionary conservation and isoform-defining sequences. *Redox Biol*. 2023;66:102851. doi:10.1016/j.redox.2023.102851
6. Vermot A, Petit-Härtlein I, Smith SME, Fieschi F. NADPH oxidases (NOX): an overview from discovery, molecular mechanisms to physiology and pathology. *Antioxidants (Basel)*. 2021;10:890. doi:10.3390/antiox10060890
7. Ogboo BC, Grabovyy UV, Maini A, et al. Architecture of the NADPH oxidase family of enzymes. *Redox Biol*. 2022;52:102298. doi:10.1016/j.redox.2022.102298
8. Sies H, Jones DP. Reactive oxygen species (ROS) as pleiotropic physiological signalling agents. *Nat Rev Mol Cell Biol*. 2020;21:363-383. doi:10.1038/s41580-020-0230-3
9. Sinenko SA, Starkova TY, Kuzmin AA, Tomilin AN. Physiological signaling functions of reactive oxygen species in stem cells: from flies to man. *Front Cell Dev Biol*. 2021;9:714370. doi:10.3389/fcell.2021.714370
10. Schröder K. NADPH oxidases: current aspects and tools. *Redox Biol*. 2020;34:101512. doi:10.1016/j.redox.2020.101512
11. Fiadeiro MB, Diogo JC, Silva AA, Kim YS, Cristóvão AC. NADPH oxidases in neurodegenerative disorders: mechanisms and therapeutic opportunities. *Antioxid Redox Signal*. 2024;41:522-541. doi:10.1089/ars.2023.0002
12. Amadio P, Sandrini L, Zarà M, Barbieri SS, Ieraci A. NADPH-oxidases as potential pharmacological targets for thrombosis and depression co-morbidity. *Redox Biol*. 2024;70:103060. doi:10.1016/j.redox.2024.103060
13. Taylor JP, Tse HM. The role of NADPH oxidases in infectious and inflammatory diseases. *Redox Biol*. 2021;48:102159. doi:10.1016/j.redox.2021.102159
14. Cipriano A, Viviano M, Feoli A, et al. NADPH oxidases: from molecular mechanisms to current inhibitors. *J Med Chem*. 2023;66:11632-11655. doi:10.1021/acs.jmedchem.3c00770
15. Reis J, Gorgulla C, Massari M, et al. Targeting ROS production through inhibition of NADPH oxidases. *Nat Chem Biol*. 2023;19:1540-1550. doi:10.1038/s41589-023-01457-5
16. Smith KC. *The Science of Photobiology*. 2nd ed. Plenum Press; 1989.
17. Hirota A, Kawachi Y, Itoh K, Nakamura Y, Xu X, Banno T. Ultraviolet a irradiation induces nf-e2-related factor 2 activation in dermal fibroblasts: protective role in UVA-induced apoptosis. *J Invest Dermatol*. 2005;124:825-832. doi:10.1111/j.0022-202X.2005.23670.x
18. Hernandez-Pigeon H, Jean C, Charruyer A, et al. UVA induces granzyme B in human keratinocytes through MIF: implication in extracellular matrix remodeling. *J Biol Chem*. 2007;282:8157-8164. doi:10.1074/jbc.M607436200
19. Heckmann M, Pirthauer M, Plewig G. Adhesion of leukocytes to dermal endothelial cells is induced after single-dose, but reduced after repeated doses of UVA. *J Invest Dermatol*. 1997;109:710-715. doi:10.1111/1523-1747.ep12340670
20. Guhl S, Stefaniak R, Strathmann M, et al. Bivalent effect of UV light on human skin mast cells—low-level mediator release at baseline but potent suppression upon mast cell triggering. *J Invest Dermatol*. 2005;124:453-456. doi:10.1111/j.0022-202X.2004.23523.x
21. Zhou YD, Fang XF, Cui ZJ. UVA-induced calcium oscillations in rat mast cells. *Cell Calcium*. 2009;45:18-28. doi:10.1016/j.ceca.2008.05.003
22. Li ZY, Jiang WY, Cui ZJ. An essential role of NAD(P)H oxidase 2 in UVA-induced calcium oscillations in mast cells. *Photochem Photobiol Sci*. 2015;14:414-428. doi:10.1039/c4pp00304g
23. Liu X, Shi Y, Liu R, Song K, Chen L. Structure of human phagocyte NADPH oxidase in the activated state. *Nature*. 2024;627:189-195. doi:10.1038/s41586-024-07056-1
24. Magnani F, Mattevi A. Structure and mechanisms of ROS generation by NADPH oxidases. *Curr Opin Struct Biol*. 2019;59:91-97. doi:10.1016/j.sbi.2019.03.001
25. Touyz RM, Anagnostopoulou A, Rios F, Montezano AC, Camargo LL. NOX5: molecular biology and pathophysiology. *Exp Physiol*. 2019;104:605-616. doi:10.1113/EP086204
26. Wondrak GT, Jacobson MK, Jacobson EL. Endogenous UVA-photosensitizers: mediators of skin photodamage and novel targets for skin photoprotection. *Photochem Photobiol Sci*. 2006;25:215-237. doi:10.1039/b504573h
27. Baier J, Maisch T, Maier M, Engel E, Landthaler M, Bäumler W. Singlet oxygen generation by UVA light exposure of endogenous photosensitizers. *Biophys J*. 2006;91:1452-1459. doi:10.1529/biophysj.106.082388
28. Park SL, Justiniano R, Williams JD, Cabello CM, Qiao S, Wondrak GT. The tryptophan-derived endogenous aryl hydrocarbon receptor ligand 6-formylindolo[3,2-b]carbazole is a nanomolar UVA photosensitizer in epidermal keratinocytes. *J Invest Dermatol*. 2015;135:1649-1658. doi:10.1038/jid.2014.503
29. Baumler W, Regensburger J, Knak A, FelgentraGer A, Maisch T. UVA and endogenous photosensitizers—the detection of singlet oxygen by its luminescence. *Photochem Photobiol Sci*. 2011;11:107-117. doi:10.1039/c1pp05142c
30. Justiniano R, de Faria LL, Perer J, et al. The endogenous tryptophan-derived photoproduct 6-formylindolo[3,2-b]carbazole (FICZ) is a nanomolar photosensitizer that can be harnessed for the photodynamic elimination of skin cancer cells *in vitro* and *in vivo*. *Photochem Photobiol*. 2021;97:180-191. doi:10.1111/php.13321
31. Leto TL, Morand S, Hurt D, Ueyama T. Targeting and regulation of reactive oxygen species generation by Nox family NADPH oxidases. *Antioxid Redox Signal*. 2009;11:2607-2619. doi:10.1089/ars.2009.2637
32. Pendyala S, Natarajan V. Redox regulation of NOX proteins. *Respir Physiol Neurobiol*. 2010;174:265-271. doi:10.1016/j.resp.2010.09.016
33. Brandes RP, Weissmann N, Schroder K. NOX family NADPH oxidases in mechano-transduction: mechanisms and consequences. *Antioxid Redox Signal*. 2014;20:887-898. doi:10.1089/ars.2013.5414
34. Naish E, Wood AJ, Stewart AP, et al. The formation and function of the neutrophil phagosome. *Immunol Rev*. 2023;314:158-180. doi:10.1111/imr.13173
35. Cui ZJ, Matthews EK. Photodynamic modulation of cellular function. *Acta Pharmacol Sin*. 1998;19:297-303.
36. Allison RR, Sibata CH. Photodynamic therapy: mechanism of action and role in the treatment of skin disease. *G Ital Dermatol Venereol*. 2010;145:491-507.
37. Fernandez JM, Bilgin MD, Grossweiner LI. Singlet oxygen generation by photodynamic agents. *J Photochem Photobiol B Biol*. 1997;37:131-140. doi:10.1016/S1011-1344(96)07349-6

38. Josefsen LB, Boyle RW. Photodynamic therapy: novel third-generation photosensitizers one step closer? *Br J Pharmacol*. 2008;154:1-3. doi:10.1038/bjp.2008.98
39. Pimenta FM, Jensen RL, Breitenbach T, Etzerodt M, Ogilby PR. Oxygen-dependent photochemistry and photophysics of "miniSOG", a protein-encased flavin. *Photochem Photobiol*. 2013;89:1116-1126. doi:10.1111/php.12111
40. Rodríguez-Pulido A, Cortajarena AL, Torra J, Ruiz-González R, Nonell S, Flors C. Assessing the potential of photosensitizing flavoproteins as tags for correlative microscopy. *Chem Commun (Camb)*. 2016;52:8405-8408. doi:10.1039/c6cc03119f
41. Torra J, Lafaye C, Signor L, et al. Tailing miniSOG: structural bases of the complex photophysics of a flavin-binding singlet oxygen photosensitizing protein. *Sci Rep*. 2019;9:2428. doi:10.1038/s41598-019-38955-3
42. An YP, Xiao R, Cui H, Cui ZJ. Selective activation by photodynamic action of cholecystokinin receptor in the freshly isolated rat pancreatic acini. *Br J Pharmacol*. 2003;139:872-880. doi:10.1038/sj.bjp.0705295
43. Jiang WY, Li Y, Li ZY, Cui ZJ. Permanent photodynamic cholecystokinin 1 receptor activation—dimer-to-monomer conversion. *Cell Mol Neurobiol*. 2018a;38:1283-1292. doi:10.1007/s10571-018-0596-3
44. Jiang HN, Li Y, Jiang WY, Cui ZJ. Cholecystokinin 1 receptor—a unique G protein-coupled receptor activated by singlet oxygen (*GPCR-ABSO*). *Front Physiol*. 2018b;9:497. doi:10.3389/fphys.2018.00497
45. Li Y, Cui ZJ. Photodynamic activation of cholecystokinin 1 receptor with different genetically encoded protein photosensitizers and from varied subcellular sites. *Biomolecules*. 2020a;10:1423. doi:10.3390/biom10101423
46. Li Y, Cui ZJ. NanoLuc bioluminescence-driven photodynamic activation of cholecystokinin 1 receptor with genetically-encoded protein photosensitizer miniSOG. *Int J Mol Sci*. 2020b;21:3763. doi:10.3390/ijms21113763
47. Jiang LL, Xie XB, Zhang L, et al. Activation of the G protein-coupled sulfakinin receptor inhibits blood meal intake in the mosquito *Aedes aegypti*. *FASEB J*. 2024;38:e23864. doi:10.1096/fj.202401165R
48. Valencia A, Kochevar IE. Nox1-based NADPH oxidase is the major source of UVA-induced reactive oxygen species in human keratinocytes. *J Invest Dermatol*. 2008;128:214-222. doi:10.1038/sj.jid.5700960
49. Kawano A, Hayakawa A, Kojima S, Tsukimoto M, Sakamoto H. Purinergic signaling mediates oxidative stress in UVA-exposed THP-1 cells. *Toxicol Rep*. 2015;2:391-400. doi:10.1016/j.toxrep.2015.01.015
50. Wu S, Gao J, Dinh QT, Chen C, Fimmel S. IL-8 production and AP-1 transactivation induced by UVA in human keratinocytes: roles of D-alpha-tocopherol. *Mol Immunol*. 2008;45:2288-2296. doi:10.1016/j.molimm.2007.11.019
51. Cooper KL, Liu KJ, Hudson LG. Enhanced ROS production and redox signaling with combined arsenite and UVA exposure: contribution of NADPH oxidase. *Free Radic Biol Med*. 2009;47:381-388. doi:10.1016/j.freeradbiomed.2009.04.034
52. Bedard K, Jaquet V, Krause KH. NOX5: from basic biology to signaling and disease. *Free Radic Biol Med*. 2012;52:725-734. doi:10.1016/j.freeradbiomed.2011.11.023
53. Raad H, Mouawia H, Hassan H, et al. The protein kinase A negatively regulates reactive oxygen species production by phosphorylating $gp91^{phox}$/NOX2 in human neutrophils. *Free Radic Biol Med*. 2020;160:19-27. doi:10.1016/j.freeradbiomed.2020.07.021
54. Preuss AK, Connor JA, Vogel H. Transient transfection induces different intracellular calcium signaling in CHO K1 versus HEK 293 cells. *Cytotechnology*. 2000;33:139-145. doi:10.1023/A:1008150402616
55. Jagnandan D, Church JE, Bánfi B, Stuehr DJ, Marrero MB, Fulton DJR. Novel mechanism of activation of NADPH oxidase 5 - calcium sensitization via phosphorylation. *J Biol Chem*. 2007;282:6494-6507. doi:10.1074/jbc.M608966200
56. Serrander L, Jaquet V, Bedard K, et al. NOX5 is expressed at the plasma membrane and generates superoxide in response to protein kinase C activation. *Biochimie*. 2007;89:1159-1167. doi:10.1016/j.biochi.2007.05.004
57. Kawahara T, Lambeth JD. Phosphatidylinositol (4,5)-bisphosphate modulates Nox5 localization via an N-terminal polybasic region. *Mol Biol Cell*. 2008;19:4020-4031. doi:10.1091/mbc.e07-12-1223
58. Reis J, Massari M, Marchese S, et al. A closer look into NADPH oxidase inhibitors: validation and insight into their mechanism of action. *Redox Biol*. 2020;32:101466. doi:10.1016/j.redox.2020.101466
59. Ott VL, Cambier JC. Activating and inhibitory signaling in mast cells: new opportunities for therapeutic intervention? *J Allergy Clin Immunol*. 2000;106:429-440. doi:10.1067/mai.2000.109428
60. Cui ZJ, Kanno T. Photodynamic triggering of calcium oscillation in the isolated rat pancreatic acini. *J Physiol*. 1997;504:47-55. doi:10.1111/j.1469-7793.1997.047bf.x
61. Barnett ME, Baran TM, Foster TH, Wojtovich AP. Quantification of light-induced miniSOG superoxide production using the selective marker, 2-hydroxyethidium. *Free Radic Biol Med*. 2018;116:134-140. doi:10.1016/j.freeradbiomed.2018.01.014
62. Jiang HN, Li Y, Cui ZJ. Photodynamic physiology—photonanomanipulations in cellular physiology with protein photosensitisers. *Front Physiol*. 2017;8:191. doi:10.3389/fphys.2017.00191
63. Li Y, Cui ZJ. Photodynamic activation of the cholecystokinin 1 receptor with tagged genetically encoded protein photosensitizers: optimizing the tagging patterns. *Photochem Photobiol*. 2022a;98:1215-1228. doi:10.1111/php.13611
64. Wyer JA, Brøndsted Nielsen S. Absorption in the Q-band region by isolated ferric $heme^{+}$ and $heme^{+}$(histidine) *in vacuo*. *J Chem Phys*. 2010;133:084306. doi:10.1063/1.3474998
65. Nakabayashi T, Islam MS, Ohta N. Fluorescence decay dynamics of flavin adenine dinucleotide in a mixture of alcohol and water in the femtosecond and nanosecond time range. *J Phys Chem B*. 2010;114:15254-15260. doi:10.1021/jp1063066
66. Steigenberger S, Terjung F, Grossart HP, Reuter R. Blue-fluorescence of NADPH as an indicator of marine primary production. *EARSeL eProc*. 2004;3:18-25. Accessed August 15 2024. http://eproceedings.uni-oldenburg.de/website/vol03_1/03_1_steigenberger1.pdf
67. Yoshimura T, Fujii S, Kamada H, et al. Spectroscopic characterization of nitrosylheme in nitric oxide complexes of ferric and ferrous cytochrome c' from photosynthetic bacteria. *Biochim Biophys Acta*. 1996;1292:39-46. doi:10.1016/0167-4838(95)00187-5

68. Grasberger H, Refetoff S. Identification of the maturation factor for dual oxidase. Evolution of an eukaryotic operon equivalent. *J Biol Chem*. 2006;281:18269-18272. doi:10.1074/jbc.C600095200
69. Kochevar IE. Singlet oxygen signaling: from intimate to global. *Sci STKE*. 2004;2004:pe7. doi:10.1126/stke.2212004pe7
70. Cló E, Snyder JW, Ogilby PR, Gothelf KV. Control and selectivity of photosensitized singlet oxygen production: challenges in complex biological systems. *Chembiochem*. 2007;8:475-481. doi:10.1002/cbic.200600454
71. Bresolí-Obach R, Torra J, Zanocco RP, Zanocco AL, Nonell S. Singlet oxygen quantum yield determination using chemical acceptors. *Methods Mol Biol*. 2021;2202:165-188. doi:10.1007/978-1-0716-0896-8_14
72. Robertson CA, Evans DH, Abrahamse H. Photodynamic therapy (PDT): a short review on cellular mechanisms and cancer research applications for PDT. *J Photochem Photobiol B*. 2009;96:1-8. doi:10.1016/j.jphotobiol.2009.04.001
73. Kessel D. Death pathways associated with photodynamic therapy. *Photochem Photobiol*. 2021;97:1101-1103. doi:10.1111/php.13436
74. Fulton DJ. Nox5 and the regulation of cellular function. *Antioxid Redox Signal*. 2009;11:2443-2452. doi:10.1089/ars.2009.2587
75. Fradin T, Bechor E, Berdichevsky Y, Dahan I, Pick E. Binding of $p67^{phox}$ to Nox2 is stabilized by disulfide bonds between cysteines in the ^{369}Cys-Gly-Cys^{371} triad in Nox2 and in $p67^{phox}$. *J Leukoc Biol*. 2018;104:1023-1039. doi:10.1002/JLB.4A0418-173R
76. Dahan I, Smith SM, Pick E. A Cys-Gly-Cys triad in the dehydrogenase region of Nox2 plays a key role in the interaction with p67phox. *J Leukoc Biol*. 2015;98:859-874. doi:10.1189/jlb.4A0315-107R
77. Guzik TJ, Chen W, Gongora MC, et al. Calcium-dependent NOX5 nicotinamide adenine dinucleotide phosphate oxidase contributes to vascular oxidative stress in human coronary artery disease. *J Am Coll Cardiol*. 2008;52:1803-1809. doi:10.1016/j.jacc.2008.07.063
78. Hahn NE, Meischl C, Kawahara T, et al. NOX5 expression is increased in intramyocardial blood vessels and cardiomyocytes after acute myocardial infarction in humans. *Am J Pathol*. 2012;180:2222-2229. doi:10.1016/j.ajpath.2012.02.018
79. Zhu C, Yu ZB, Chen XH, Ji CB, Qian LM, Han SP. DNA hypermethylation of the NOX5 gene in fetal ventricular septal defect. *Exp Ther Med*. 2011;2:1011-1015. doi:10.3892/etm.2011.294
80. Hong J, Resnick M, Behar J, et al. Acid-induced p16 hypermethylation contributes to development of esophageal adenocarcinoma via activation of NADPH oxidase NOX5-S. *Am J Physiol Gastrointest Liver Physiol*. 2010;299:G697-G706. doi:10.1152/ajpgi.00186.2010
81. Brieger K, Schiavone S, Miller FJ Jr, Krause KH. Reactive oxygen species: from health to disease. *Swiss Med Wkly*. 2012;142:w13659. doi:10.4414/smw.2012.13659
82. Ohye H, Sugawara M. Dual oxidase, hydrogen peroxide and thyroid diseases. *Exp Biol Med (Maywood)*. 2010;235:424-433. doi:10.1258/ebm.2009.009241
83. El Hassani RA, Benfares N, Caillou B, et al. Dual oxidase2 is expressed all along the digestive tract. *Am J Physiol Gastrointest Liver Physiol*. 2005;288:G933-G942. doi:10.1152/ajpgi.00198.2004
84. Luxen S, Belinsky SA, Knaus UG. Silencing of DUOX NADPH oxidases by promoter hypermethylation in lung cancer. *Cancer Res*. 2008;68:1037-1045. doi:10.1158/0008-5472.CAN-07-5782
85. Geiszt M, Witta J, Baffi J, Lekstrom K, Leto TL. Dual oxidases represent novel hydrogen peroxide sources supporting mucosal surface host defense. *FASEB J*. 2003;17:1502-1504. doi:10.1096/fj.02-1104fje
86. Sarr D, Tóth E, Gingerich A, Rada B. Antimicrobial actions of dual oxidases and lactoperoxidase. *J Microbiol*. 2018;56:373-386. doi:10.1007/s12275-018-7545-1
87. Cui C, Jiang M, Jain N, et al. Structural basis of human NOX5 activation. *Nat Commun*. 2024;15:3994. doi:10.1038/s41467-024-48467-y
88. Petit-Hartlein I, Vermot A, Thepaut M, et al. X-ray structure and enzymatic study of a bacterial NADPH oxidase highlight the activation mechanism of eukaryotic NOX. *elife*. 2024;13:RP93759. doi:10.7554/eLife.93759
89. Liu Z. Antioxidant activity of the thioredoxin system. *Biophys Rep*. 2023;9:26-32. doi:10.52601/bpr.2023.230002
90. Chen Q, Liu W, Sun X, Liu KJ, Pan R. Endogenous reactive oxygen species and nitric oxide have opposite roles in regulating HIF-1alpha expression in hypoxic astrocytes. *Biophys Rep*. 2021;7:239-249. doi:10.52601/bpr.2021.200016
91. Wu JX, Liu R, Song K, Chen L. Structures of human dual oxidase 1 complex in low-calcium and high-calcium states. *Nat Commun*. 2021;12:155. doi:10.1038/s41467-020-20466-9

SUPPORTING INFORMATION

Additional supporting information can be found online in the Supporting Information section at the end of this article.

How to cite this article: Xie XB, Shu Y, Cui ZJ. To activate NAD(P)H oxidase with a brief pulse of photodynamic action. *The FASEB Journal*. 2024;38:e70246. doi:10.1096/fj.202402292R